

CIPANP2015-Gray
FERMILAB-CONF-15-402-E
November 7, 2018

Muon $g-2$ Experiment at Fermilab

FREDERICK GRAY¹

*Department of Physics and Astronomy
Regis University, Denver, CO 80221, USA*

A new experiment at Fermilab will measure the anomalous magnetic moment of the muon with a precision of 140 parts per billion (ppb). This measurement is motivated by the results of the Brookhaven E821 experiment that were first released more than a decade ago, which reached a precision of 540 ppb. As the corresponding Standard Model predictions have been refined, the experimental and theoretical values have persistently differed by about 3 standard deviations. If the Brookhaven result is confirmed at Fermilab with this improved precision, it will constitute definitive evidence for physics beyond the Standard Model. The experiment observes the muon spin precession frequency in flight in a well-calibrated magnetic field; the improvement in precision will require both 20 times as many recorded muon decay events as in E821 and a reduction by a factor of 3 in the systematic uncertainties. This paper describes the current experimental status as well as the plans for the upgraded magnet, detector and storage ring systems that are being prepared for the start of beam data collection in 2017.

PRESENTED AT

Twelfth Conference on the Intersections
of Particle and Nuclear Physics
Vail, Colorado, U.S.A., May 19, 2015

¹On behalf of the Fermilab E989 Muon $g-2$ Collaboration

1 Introduction

The Fermilab E989 Collaboration is constructing a new experiment to measure the muon’s anomalous magnetic moment, a_μ , with a precision of 140 parts per billion (ppb). This quantity was last measured by the E821 Collaboration at Brookhaven National Laboratory [1]. That experiment reached a final precision of 540 ppb after combining runs with positive [2] and negative [3] muons, which were measured to 730 and 720 ppb, respectively. As shown in Figure 1, the results disagree by more than three standard deviations with recent evaluations of the theoretical prediction of the Standard Model. While it is not yet definitive, the discrepancy strongly suggests that there may be effects on the muon’s magnetic moment from particles or interactions that are not included in the Standard Model.

The potential for a discovery of new physics provides motivation for the improved measurement of a_μ at Fermilab. Table 1 summarizes the planned improvements in statistical and systematic errors. Some major systems are being redesigned completely for higher precision, although a number of major components from E821 are being refurbished and reused, particularly the superconducting magnet. The collaboration includes some veterans of E821, but the number of new members is much larger, so the experiment will effectively provide an independent new measurement.

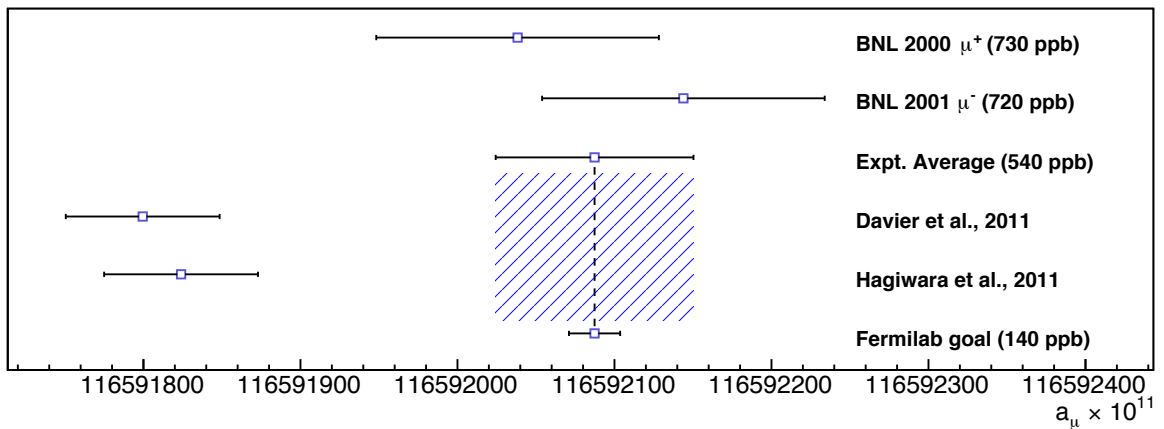


Figure 1: Comparison of the Brookhaven E821 results and the projected sensitivity of the Fermilab E989 Muon $g-2$ experiment to current theoretical calculations, showing a discrepancy of more than 3σ that could potentially be due to new physics beyond the Standard Model.

| | E821 μ^+ | E821 μ^- | Fermilab target |
|---|--------------|--------------|-----------------|
| Statistics | 620 | 670 | 100 |
| Systematics in ω_a | 310 | 210 | 70 |
| - <i>Overlapping pulses (pile-up)</i> | 130 | 80 | 40 |
| - <i>Coherent betatron oscillations</i> | 210 | 70 | 30 |
| - <i>Detector gain changes</i> | 130 | 120 | 20 |
| - <i>Muon losses</i> | 100 | 90 | 20 |
| - <i>Others</i> | 90 | 100 | 40 |
| Systematics in ω_p | 240 | 170 | 70 |
| Total (quadrature sum) | 730 | 720 | 140 |

Table 1: Projected improvements in statistical and systematic uncertainties, in parts per billion.

The determination of the theoretical value of $a_\mu = \frac{1}{2}(g - 2)$ is described in detail in References [4, 5]. The Dirac equation predicts that $g = 2$, so a nonzero value for a_μ arises from coupling to virtual particles. The vast majority (99.6%) of the value of a_μ arises from the leading-order quantum electrodynamics (QED) process that involves the exchange of a single virtual photon, and higher-order QED contributes nearly all of the rest. However, there is essentially no uncertainty associated with these contributions; the uncertainty from the hadronic contributions is dominant.

Approximately three-quarters of the squared uncertainty comes from hadronic vacuum polarization, which is determined primarily from a dispersion integral using hadron production cross section data from e^+e^- collisions. New results from BES-III on the dominant $e^+e^- \rightarrow \pi^+\pi^-$ process are now available [6], and additional measurements with the VEPP-2000 collider in Novosibirsk are anticipated [7]. The remaining error arises from hadronic light-by-light scattering, which has historically required nuclear modeling techniques. However, work is in progress to calculate it using Lattice QCD [8] and with a dispersive approach [9]. Consequently, the precision of the Standard Model value may improve to about 250 ppb based on work that is already in progress, compared with an uncertainty of 420 ppb today.

The discrepancy of more than three standard deviations could be explained by a loop diagram describing new particles or interactions. Although supersymmetry is increasingly constrained by its absence at the LHC experiments, it still remains a viable candidate to account for the discrepancy [10, 11]. As an alternative, additional $U(1)$ gauge bosons known as “dark photons” were frequently discussed; however, they have now been almost excluded as the explanation for the entire anomaly [12].

The principle of the experiment is to observe the anomalous precession frequency ω_a as a bunched beam of polarized muons circulates in an applied magnetic field. This frequency is the difference between the rotation frequencies of the muons’ spin and momentum, and it equals $a_\mu(\frac{e}{m})B$. Parity violation causes the high-energy positrons produced in μ^+ decay to preferentially follow the muon spin direction, so the number of positrons that are detected by electromagnetic calorimeters with energy above a defined threshold is modulated at ω_a . This modulation frequency is measured with high precision, as is the free proton NMR frequency ω_p that indicates the magnetic field. The anomalous magnetic moment is then calculated as $R/(\lambda - R)$ from the ratio of frequencies $R = \omega_a/\omega_p$ and the corresponding ratio of magnetic moments $\lambda = \mu_\mu/\mu_p$.

The storage ring magnet used in E821 was relocated from Brookhaven to Fermilab in June and July 2013, and it has now been successfully powered in its new location. The circular magnet has a C-shaped cross section and consists of a steel yoke and precisely-ground pole pieces that are excited by four superconducting niobium-titanium coils; it operates at a field of 1.45 T. At a “magic” muon momentum of 3.09 GeV/c, the spin precession frequency is unaffected by electric fields, allowing a large (several kV/cm) electric quadrupole field to be used to confine the beam vertically.

The equilibrium radius of the beam at this momentum is 7.112 m, and the dilated lifetime is 64.4 μs . Each orbit around the ring requires 149 ns, and the anomalous precession period is 4.37 μs .

2 Beam and Injection

The precision of the E821 measurement was limited primarily by statistics. The target of the new experiment is a statistical precision of 100 ppb, which will require 1.6×10^{11} accepted muon decay events. Consequently, a plan has been developed to provide a high-intensity muon beam to the experiment.

The Booster at Fermilab delivers 8 GeV protons to the Recycler, where they will be restructured into 16 bunches per 1.33 s supercycle. Each bunch will have a full width of ± 62 ns. This primary beam will be extracted onto the AP0 target with a separation of 10 ms between bunches. Pions will be collected from the target using a pulsed lithium lens, and the pion beam will be transported to the Delivery Ring, which previously served as the antiproton debuncher in the Tevatron era. Three orbits around this ring will provide an extended path for pions to decay in flight into muons, as well as an opportunity to separate the pions and muons from proton contamination by time-of-flight. In all, the pion decay path is more than 2 km long, so the result will be essentially a pure muon beam.

The beam will enter the storage ring through a superconducting inflector that cancels the main magnet's field. The inflector, refurbished from E821, is a long, narrow pipe with a channel that is $9 \times 28 \text{ mm}^2 \times 1.7$ m. Design studies are in progress for a possible new inflector with a larger aperture. The beam will then be kicked onto a stored orbit by fast kicker magnets driven by a Blumlein pulse forming network. Unlike the E821 kicker, which required two turns to fully kick the beam, the new system will deliver the entire deflection in the first turn. This kick will populate the phase space of the ring more fully and will allow the beam to be collimated more completely, reducing muon losses at later times in the fill.

The injection process will be optimized not only to reach the maximum stored intensity, but also to populate the ring's phase space as uniformly and symmetrically as possible. Coherent betatron oscillations arise from the rotation of the phase space over time at each azimuthal location. They are observed as modulations of the centroid position and the width of the beam. In E821, the frequency of these oscillations was nearly $2\omega_a$, which directly biased the fit for ω_a . To move significantly above this dangerous frequency, the electric quadrupole system is being upgraded to support voltages of 32 kV rather than 24 kV.

Validated models of the beamline and injection process have been developed using BMAD and GEANT4. They predict 7×10^5 muons per fill at the end of the beamline, with a full momentum width $\Delta p/p$ of $\pm 2.5\%$. This is substantially larger than the

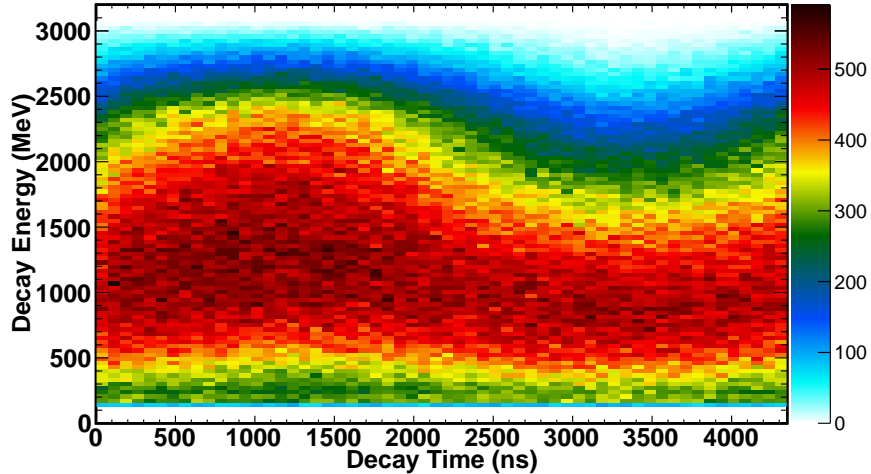


Figure 2: Positron energy spectrum as a function of time, shown for one anomalous precession period. (Reproduced from [13].)

ring acceptance of $\pm 0.15\%$, so about 2×10^4 muons per fill will be stored, leading to 1×10^3 accepted muon decay events with detected positron energies exceeding the threshold. Consequently, it will be possible to collect the required statistics within about a year of running time.

3 Detectors and electronics

As the muon decays by $\mu^+ \rightarrow e^+ + \nu_e + \bar{\nu}_\mu$, parity violation in the weak interaction causes high-energy positrons to follow the muon spin direction. This correlation is most easily seen by examining limiting cases in the CM frame; consider that the highest-energy positrons recoil back-to-back against the neutrino and antineutrino. Their fixed helicities mean that they have zero net spin, so the positron must maintain the muon's initial spin. The effect is then accentuated in the transformation to the laboratory frame, where the forward-going positrons receive an additional forward boost. The modulation of the expected positron energy spectrum as the muon spin rotates is shown in Figure 2.

In the traditional analysis, a threshold is set at 1.86 GeV, and the number of positrons exceeding this threshold is recorded. This choice of threshold maximizes the statistical figure of merit $\sqrt{N}A$, where A is the modulation asymmetry. Other analysis methods are possible, and in some cases they have different systematic uncertainties. In one such method, the total deposited energy is recorded as a function of time; energy-binned and asymmetry-weighted analysis methods can also be explored.

The positrons will be detected by 24 electromagnetic calorimeter stations spaced equally around the ring. These stations have been designed to minimize the systematic error from “pile-up” of overlapping pulses from multiple positron hits. Because higher-energy positrons follow a larger-radius arc to the calorimeter, they have a longer time of flight from the decay point, and therefore they carry a different anomalous spin precession phase from lower-energy positrons. The probability of mistaking two lower-energy positrons for a single higher-energy one is rate-dependent, so it is more likely to happen early in the fill than later. This time-dependent phase is equivalent to a frequency shift.

Consequently, the calorimeters will be optimized for separation of multiple-positron events in both space and time [14]. For spatial resolution, they will be segmented into a 9×6 array of lead fluoride (PbF_2) crystals. Logistically, this segmentation requires that the crystals be instrumented with very compact photodetectors, so Hamamatsu silicon multi-pixel photon counters (MPPC) will be used instead of traditional photomultiplier tubes (PMT). The MPPCs are not affected by large magnetic fields, so they do not require the long lightguides that would be needed to locate PMTs away from the magnet. Light in PbF_2 is produced by the Cerenkov effect, so the width of the pulse in time is much faster than in a scintillation-based detector; a width of 3 ns (FWHM) has been demonstrated.

To take advantage of the fast pulses, new waveform digitizers are being constructed. They will provide 12-bit sampling of each crystal independently at a rate of 800 MSPS, and they will transfer their data to an online computing facility using 10 GB/s Ethernet. Every voltage sample from each fill will be available to the computer, which will use graphics processing units (GPU) as vector processors to extract the times and energies to be recorded. This data acquisition system [15] will allow the flexibility to implement several analysis methods.

Any time dependence during the fill in the energy response of the detectors will also lead directly to a systematic error. A gain monitoring system [16] has been developed; it will distribute laser pulses via a network of splitters and optical fibers to each calorimeter segment and to stable monitoring detectors. This technique has been demonstrated to allow measurements of the detector gain to better than 0.1% over the time scale of one fill of the storage ring.

New straw-tube tracking chambers will be placed at two locations in the ring. Each will consist of eight U-V straw planes that will allow positrons to be tracked back to the decay vertex. The primary role for the trackers is to measure the muon distribution to use as a weighting in the determination of the average magnetic field. It will also be used to search for a muon electric dipole moment, which would appear as a modulation of the vertical component of the decay positron momentum. It will also allow the calorimeter to be tested with particles of known momentum and with identified pile-up events, and it will allow the distribution of lost muons to be characterized.

There will also be a set of four scintillating fiber beam monitors that can be plunged into the storage region to measure the beam profile in both x and y at two locations in the ring, at 180° and 270° from the injection point. Scintillating fiber monitors are also being designed for installation at the entrance and exit of the inflector. All of these devices can be used to optimize and monitor the beam injection.

4 Magnetic field

The magnetic field is measured using NMR probes, which are calibrated in terms of the free proton precession frequency ω_p . The field will be continuously monitored by more than 300 fixed probes placed outside the vacuum chambers. These fixed probes will be calibrated every few days to a set of 17 probes housed on an in-vacuum trolley. The trolley will in turn be regularly calibrated against an absolute standard probe; a spherical H₂O-filled probe exists, and an absolute calibration based on ³He is being developed.

The target for the uncertainty in ω_p is 70 ppb, a factor of 3 improvement from the level reached in E821. To reach this target will require careful shimming of the magnet, to better than 100 ppb in each multipole. The stability of the magnet is expected to be excellent in the new MC-1 experimental hall, which has a single-segment concrete floor and which will provide temperature regulation at the $\pm 2^\circ$ F level. Trolley runs will be taken more frequently than in E821, and its azimuthal position resolution will be improved by a factor of 2. The free-induction decay waveforms from all of the fixed probes will be recorded, and the temperature dependence of the probes will be calibrated directly.

5 Progress and schedule after CIPANP 2015

At the time of the conference, the reassembly of the storage ring magnet at Fermilab was nearly complete. Only a few final details had to be resolved before the magnet could be cooled to 4 K and powered. The final beamline magnets were moved into place in preparation for field shimming, and civil construction of the external beamline enclosures was under way.

In late June, the magnet was successfully ramped up to a current of 3400 A. However, an unexpectedly high resistance was measured in one of the lead cans, requiring that it be re-opened for repair. Following this repair, the storage ring current reached 5300 A on September 22, demonstrating a safety margin above the normal operating current of 5100 A that produces a 1.45 T field. Consequently, the magnet is now prepared for shimming to begin. A first scan, conducted immediately after the first power-up to full current and without any adjustments, showed that

azimuthal variations in the field were only one order of magnitude larger than in the final field map from E821.

Shimming activity is expected to last until March 2016; at the same time, other systems are being prepared for installation: the vacuum chambers, the inflector, the kicker, the focusing quadrupoles, and all of the field-measuring equipment. The vacuum chambers are expected to be installed in April and May 2016, with the remaining installations of ring-integrated systems following in the summer and fall. This schedule will provide a period of testing while construction is completed on the accelerator and beamline systems. The first commissioning of the experiment with beam is expected in March 2017, with production data to begin in September after a planned summer shutdown. It is certainly possible that a first result will be available in time for CIPANP 2018.

ACKNOWLEDGMENTS

The author would like to thank the conference organizers for all of their work; they made CIPANP 2015 an informative and enjoyable event with old and new colleagues. The experiment is supported in part by the U.S. Department of Energy and the National Science Foundation. Fermilab is operated by Fermi Research Alliance, LLC under contract number DE-AC02-07CH11359 with the U.S. Department of Energy. The author's participation at CIPANP 2015 was supported by the National Science Foundation under grant number PHY-1206039.

References

- [1] G. W. Bennett *et al.* [Muon g-2 Collaboration], Phys. Rev. D **73**, 072003 (2006), [hep-ex/0602035].
- [2] G. W. Bennett *et al.* [Muon g-2 Collaboration], Phys. Rev. Lett. **89**, 101804 (2002), [hep-ex/0208001].
- [3] G. W. Bennett *et al.* [Muon g-2 Collaboration], Phys. Rev. Lett. **92**, 161802 (2004), [hep-ex/0401008].
- [4] M. Davier, A. Hoecker, B. Malaescu and Z. Zhang, Eur. Phys. J. C **71**, 1515 (2011), Eur. Phys. J. C **72**, 1874 (2012), arXiv:1010.4180 [hep-ph].
- [5] K. Hagiwara, R. Liao, A. D. Martin, D. Nomura and T. Teubner, J. Phys. G **38**, 085003 (2011), arXiv:1105.3149 [hep-ph].
- [6] M. Ablikim *et al.* [BESIII Collaboration], arXiv:1507.08188 [hep-ex].

- [7] Y. A. Rogovsky *et al.*, Phys. Part. Nucl. Lett. **11**, no. 5, 651 (2014).
- [8] L. Jin, T. Blum, N. Christ, M. Hayakawa, T. Izubuchi and C. Lehner, arXiv:1509.08372 [hep-lat].
- [9] V. Pauk and M. Vanderhaeghen, Phys. Rev. D **90**, no. 11, 113012 (2014), arXiv:1409.0819 [hep-ph].
- [10] H. G. Fargnoli, C. Gwendiger, S. Passehr, D. Stöckinger and H. Stöckinger-Kim, Phys. Lett. B **726** (2013) 717, arXiv:1309.0980 [hep-ph].
- [11] M. Bach, J. H. Park, D. Stöckinger and H. Stöckinger-Kim, arXiv:1504.05500 [hep-ph].
- [12] J. R. Batley *et al.* [NA48/2 Collaboration], Phys. Lett. B **746**, 178 (2015), arXiv:1504.00607 [hep-ex].
- [13] J. Grange *et al.* [Muon g-2 Collaboration], arXiv:1501.06858 [physics.ins-det].
- [14] A. T. Fienberg *et al.*, Nucl. Instrum. Meth. A **783**, 12 (2015), arXiv:1412.5525 [physics.ins-det].
- [15] W. Gohn, arXiv:1506.00608 [physics.ins-det].
- [16] A. Anastasi *et al.*, Nucl. Instrum. Meth. A **788**, 43 (2015), arXiv:1504.00132 [physics.ins-det].